Structure of Yeast Poly(A) Polymerase in Complex with a Peptide from Fip1, an Intrinsically Disordered Protein[†,‡]

Gretchen Meinke,[§] Chukwudi Ezeokonkwo,[§] Paul Balbo,[§] Walter Stafford,[||] Claire Moore,[§] and Andrew Bohm*[,§]

Department of Biochemistry, Tufts University, 136 Harrison Avenue, Boston, Massachusetts 02111, and Boston Biomedical Research Institute, 64 Grove Street, Watertown, Massachusetts 02472

Received February 4, 2008; Revised Manuscript Received May 8, 2008

ABSTRACT: In yeast, the mRNA processing enzyme poly(A) polymerase is tethered to the much larger 3′-end processing complex via Fip1, a 36 kDa protein of unknown structure. We report the 2.6 Å crystal structure of yeast poly(A) polymerase in complex with a peptide containing residues 80−105 of Fip1. The Fip1 peptide binds to the outside surface of the C-terminal domain of the polymerase. On the basis of this structure, we designed a mutant of the polymerase (V498Y, C485R) that is lethal to yeast. The mutant is unable to bind Fip1 but retains full polymerase activity. Fip1 is found in all eukaryotes and serves to connect poly(A) polymerase to pre-mRNA processing complexes in yeast, plants, and mammals. However, the Fip1 sequence is highly divergent, and residues on both Pap1 and Fip1 at the observed interaction surface are poorly conserved. Herein we demonstrate using analytical ultracentrifugation, circular dichroism, proteolytic studies, and other techniques that, in the absence of Pap1, Fip1 is largely, if not completely, unfolded. We speculate that flexibility may be important for Fip1's function as a molecular scaffold.

Cleavage and polyadenylation of the 3′ end of mRNA is catalyzed by a collection of over a dozen proteins which assemble on the phosphorylated C-terminal domain of RNA polymerase II during transcription (*1, 2*). Within this complex, poly(A) polymerase (PAP)[1] is responsible for the poly(A) addition. PAP is a template-independent polymerase, which belongs to the pol X family. Other members of this family include DNA polymerase β, CCA adding enzyme, terminal nucleotidyl transferase, and terminal uridylyl transferase, as well as a number of bacterial enzymes which inactivate antibiotics through nucleotidyl transfer (*3*). Crystal structures of yeast and bovine PAP have demonstrated significant structural conservation of this enzyme, even in regions where the sequence homology is weak (*4–6*). Yeast PAP, Pap1, has been solved both alone and in complex with its RNA and nucleotide substrates. These structures demonstrated that the polymerase is capable of large domain movements, and kinetic and biophysical studies indicate that these movements are required for substrate recognition and catalysis (*7–9*).

Yeast Fip1, a 36 kDa protein with no known structural domains, is the only protein shown to interact with Pap1 (*10, 11*). The protein contains an acidic region near its N-terminus and a proline-rich region near its C-terminus. Fip1 knockouts are lethal in yeast, and tandem affinity tags placed on Fip1 have been shown to pull down the large complex of proteins known as cleavage polyadenylation factor (CPF) (*12*). C-Terminal Fip1 deletions up to residue 220 have little if any effect on yeast viability or polyadenylation catalyzed by CPF (*11*). In addition to its interaction with Pap1, Fip1 has also been shown to interact directly with yeast polyadenylation factors, Pfs2 (*13*), Rna14 (*10*), and Yth1 (*14*). These data suggest that Fip1 plays a central role in stabilizing and organizing the complex. In particular, the interaction between Fip1 and Rna14 is thought to link the two large subcomplexes within the 3′-end processing machinery: CFI, which binds the upstream A-rich motif in the pre-mRNA (*15*), and CPF, which contains the poly(A) polymerase and Ysh1, the nuclease responsible for pre-mRNA cleavage (*16–18*).

Fip1 is also found in mammals, where it plays a similar, but not identical role. As in yeast, mammalian Fip1 interacts with poly(A) polymerase, CstF77 (the Rna14 homologue), and CPSF30 (a homologue of Yth1) (*19*). In higher eukaryotes, Fip1 also interacts with CPSF160 (a homologue of the yeast polyadenylation subunit Cft1) and RNA. The RNA interaction is through a highly basic, C-terminal extension not present in the yeast Fip1 sequence. This extension is also found in Fip1 genes from the plant kingdom. *Arabidopsis* Fip1 is over 800 amino acids longer than yeast Fip1 and also interacts with Pap1, Yth1, and Rna14 homologues (*20*). In addition, *Arabidopsis* Fip1 interacts with poly(A) binding protein (an interaction not observed in yeast or mammals)

[†] The work by G.M., P.B., and A.B. was supported by NIH Grant GM065972 to A.B. The work by C.E. and C.M. was supported by NIH Grant GM041752 to C.M.

[‡] The coordinates and structure factors for the complex described in this paper have been deposited to the Protein Data Bank under deposition code 3C66.

* Corresponding author. Phone: 617-636-2994. Fax: 617-636-2409. E-mail: Andrew.Bohm@tufts.edu.

[§] Tufts University.

[||] Boston Biomedical Research Institute.

[1] Abbreviations: PAP, polyadenylate polymerase; CPF, cleavage polyadenylation factor; hFip1, human Fip1; CFI, cleavage factor I; CFI_m, mammalian CFI; CYC1, iso-1-cytochrome *c* precursor RNA; Fip192, N-terminal hexahistidine-tagged Fip1 residues 1−192; Fip220, N-terminal hexahistidine-tagged Fip1 residues 1−220.

10.1021/bi800204k CCC: $40.75
Published on Web 06/07/2008

and with CFIm-25 (*20*). The latter subunit has no obvious sequence homologue in yeast, though it is functionally homologous to yeast Hrp1 in that it stabilizes the complex on the RNA substrate. In humans a similar situation exists; CFI_m is sufficient to direct sequence-specific, A(A/U)UAAA-independent polyadenylation via recruitment of poly(A) polymerase and hFip1 to the RNA substrate (*21*).

The sequence of Fip1 is highly divergent across the phyla, and the only highly conserved region (yeast residues in the 170−220 region) includes the region (206−220) involved in Yth1 binding. Fip1 has also been shown to affect the *in vitro* activity of poly(A) polymerase. In yeast, isolated Fip1 inhibits polyadenylation activity, an effect which is relieved by other polyadenylation factors (*11*). In mammals and plants isolated Fip1 has been shown to enhance polyadenylation activity (*19, 20*).

To better understand the interaction of Fip1 with Pap1, we have undertaken a series of experiments that probe the structure of Fip1 and the effect this protein has on polyadenylation. We report here the crystal structure of Pap1 in complex with a 26 amino acid peptide containing residues 80−105 of Fip1. Earlier deletion analysis has demonstrated that this region of Fip1 is necessary for *in vitro* Pap1 binding and for rescue of yeast harboring the lethal Fip1 knockout (*11*). The peptide containing the Pap1-binding domain of Fip1 will be referred to as Fip_{pbd}. We also show that longer versions of Fip1, while highly soluble, are disordered in solution. These data support a model in which only a portion of the full-length protein adopts a defined conformation upon binding Pap1, and the generally extended nature of Fip1 suggests that the connection between Pap1 and the remainder of the complex may be relatively plastic. The functional consequences of having Pap1 connected to the remainder of the complex via a flexible tether are also discussed.

EXPERIMENTAL PROCEDURES

Expression and Purification of Proteins. A C-terminal His-tagged construct of Pap1 (amino acids 1−537) (previously described as PAP△0H6) was overexpressed and purified as described (*8*). The purified protein was concentrated by ultrafiltration using Vivaspin 10000 MWCO spin concentrators (VivaSience) to ∼40 mg/mL. The protein was aliquoted, flash frozen in liquid nitrogen, and stored at −80 °C. The double mutant, V498Y C485R, was expressed and purified in the same manner as the wild-type enzyme and with similar yields. Two His-tagged constructs of FIP (residues 1−192 and residues 1−220) were also overexpressed and purified as described (*11*). These are referred to as Fip192 and Fip220 in this work.

Preparation of the Fip_{pbd} Peptides. The 26mer peptide corresponding to Fip1 residues 80−105 (referred here as Fip_{pbd}) was synthesized at the Boston Biomedical Research Institute, purified by reverse-phase HPLC, and lyophilized to dryness. The peptide was resuspended in 10 mM Tris, pH 7.5, and 50 mM NaCl. Because the peptide was insoluble in water, DMSO was added to a final concentration of 30%. The concentration of the peptide was determined based on absorbance at 280 nm and a calculated extinction coefficient. The N-terminal biotinylated Fip peptide used for the surface plasmon resonance experiment was prepared and purified by the Tufts DNA/protein core facility. The biotinylated peptide contains three amino acids (residues Ser Asp Ser, corresponding to Fip1 residues 77−79) between the biotin moiety and the Fip_{pbd} sequence.

Crystallization and Structure Determination of the Pap1−Fip_{pbd} Complex. A native gel similar to that shown in Figure 2a was used to determine the amount of Fip_{pbd} necessary to form a stoichometric complex with Pap1. The complex was prepared by diluting stock PAP 10-fold with buffer 1 (10 mM Tris, pH 7.5, 50 mM NaCl, 10% glycerol, 1 mM DTT) to a final concentration of ∼5 mg/mL. The stock Fip_{pbd} peptide was diluted 10-fold to a final concentration of ∼2.9 mg/mL. The diluted Fip_{pbd} was slowly added to the diluted PAP for a final molar ratio of Fip_{pbd}:PAP of ∼10:1. The complex was concentrated using ultrafiltration with a Vivaspin500 (MWCO 10 PES), to a final concentration ∼8 mg/mL. The complex was aliquoted in small volumes and flash frozen in liquid nitrogen and stored at −80 °C.

Crystals were grown at 4 °C by vapor diffusion in hanging drop setups. One microliter of the Pap1/Fip_{pbd} complex was mixed with 1 μL of reservoir (100 mM MES, pH 6.5, 8−10% PEG 20000), and the drops were set over 1 mL of the reservoir solution. Rod-shaped crystals grew quickly and were harvested for data collection after a few days. Single crystals were transferred to a cryogenic solution (100 mM MES, pH 6.5, 15% PEG 20000, 25% glycerol) via a nylon loop and flash-frozen in liquid nitrogen for X-ray data analysis at cryotemperatures. Data were collected at 100 K via mail-in crystallography at NSLS beamline X29A at Brookhaven National Laboratory.

The structure was solved by molecular replacement using earlier Pap1 structures as a composite search model and the program Phaser (*22*). All the orthorhombic space groups were searched, and a unique solution was found only with the space group $P2_12_12$. The asymmetric unit contains two copies of the Pap1−Fip_{pbd} complex with a solvent content of ∼58%. The structure was refined through iterative cycles of real space building/refinement in Coot (*23*) and reciprocal space refinement in Refmac5 (*24*). During the late stages of the refinement, the model was subjected to TLS refinement (*25*). In this refinement, each Pap1−Fip1 complex was divided into four TLS units, corresponding to the three Pap1 domains and the Fip1 peptide.

Structure Analysis. Molecular surface calculations were performed using the program AREAIMOL (*26*) within CCP4i, using a probe radius of 1.4 Å. As the complex described by Pap1 molecule A and Fip1 molecule C is better ordered than that involving molecules B and D, the values reported are for the former complex. Molecular graphics figures were prepared using the program PyMOL (*27*).

Yeast Strains and Plasmids. Yeast strains used in this study are as follows: W303 (*MAT*a/*MAT* {*leu2−3, 112; trp1−1 can1−100 ura3−1 ade2−1 his3−11, 15} phi*+) (*28*), and PAP1-TAP (*MATa, ura3, leu2, trp1*). The *PAP1*Δ*10*-containing plasmid used to express rPap1 in *Escherichia coli* was described previously (*8*). The *pap1-*Δ*10,C485R/V489Y* plasmid was constructed by changing cysteine 485 to arginine and valine 489 to tyrosine by site-directed mutagenesis with the QuikChange protocol (Stratagene, La Jolla, CA). The *PAP1*Δ*10* and *pap1-*Δ*10,C485R/V489Y* cassettes were cut out of the plasmid at the *Sac*I and *Pvu*II sites and ligated to a YCp50 leucine plasmid at the same sites. The *PAP1* chromosomal deletion was made in a W303 diploid strain

by replacing one chromosomal copy of *PAP1* with *HIS3*. The heterozygous diploid cells were transformed with *PAP1* on a YCp50 uracil plasmid and haploid cells containing the *PAP1* deletion and the covering plasmid obtained by sporulation using standard procedures (*29*). The *PAP1*Δ*10* and *pap1-*Δ*10,C485R/V489Y* strains were made by transforming the plasmids into the haploid W303 strain and selecting for growth on synthetic Complete media minus leucine and uracil (CM − Leu, Ura). 5FOA plates contained 1 mg/mL 5-fluoroorotic acid in synthetic Complete medium. The *PAP1*Δ*10* and *pap1-*Δ*10,C485R/V489Y* plasmids were also transformed into the PAP1-TAP strain to examine protein expression.

Extract Preparation and Western Blotting. PAP1-TAP strains containing the *PAP1*Δ*10* or *pap1-*Δ*10,C485R/V489Y* plasmids were grown overnight in CM − Leu media at 30 °C with shaking. The cells were harvested by centrifugation at 5000 rpm for 5 min and resuspended in buffer A (10 mM HEPES-KOH, pH 7.8, 1.5 mM $MgCl_2$, 10 mM KCl, 0.5 mM dithiothreitol (DTT), 1 mM phenylmethanesulfonyl fluoride, 0.6 μM leupeptin, and 2 μL of pepstatin A). The cells were disrupted with an equal volume of sterile glass beads (0.5 mm diameter) by four cycles of 1 min vortexing, with 1 min of cooling on ice between cycles. The extract was cleared by centrifugation at 2*g* for 2 min at 4 °C. Additional insoluble material was removed by centrifugation at 10000*g* for 30 min at 4 °C. Western blotting was performed with these extracts using standard protocols, and proteins were detected by using a monoclonal Pap1 antibody (*30*).

Biochemical and Biophysical Analyses of Fip1 and Pap1/Fip1 Complexes. Gel filtration was performed using a Sephacryl S-200 HR (Amersham) column under a variety of buffer conditions. The results were insensitive to changes in pH in the 6.5−8.5 range and changes in salt concentration from 100 to 500 mM. Calibration curves used to determine the observed molecular masses of Fip1 and Pap1 samples were generated using gel filtration standards from Bio-Rad. Dynamic light scattering measurements were taken using a PD2000 instrument from Precision Detectors (Bellingham, MA). The experiments were carried out at room temperature at pH 7.5 and in the presence of 100 mM NaCl. Analytical ultracentrifugation experiments were performed using interference optics on a BeckmanCoulter XL-I analytical ultracentrifuge at 50000 rpm and at a temperature of 20 °C. The Fip220 protein was dialyzed overnight against 100 mM NaCl and 100 mM Tris, pH 7.5, prior to the run. The data were analyzed using the software program SEDANAL (*31*) to compute normalized time derivative $g(s^*)$ curves. The sedimentation coefficient and the molar mass were determined with SEDANAL by fitting globally to a single component model over four concentrations ranging from 0.044 to 1.15 mg/mL. The errors are expressed as 95% confidence limits and were computed using *F*-statistics. A partial specific volume of 0.731 cm^3/g and a hydration of 0.4876 g of water/g of protein were computed from the amino acid composition using the software program SEDNTRP (*32*). Limited proteolysis was carried out as follows: For the Fip1 alone digests, concentrated Fip220 was diluted to 0.5 mg/mL with 20 mM Tris, pH 7.5, 10% glycerol, 100 mM NaCl, 1 mM $CaCl_2$, and 1 mM $MgCl_2$. Trypsin and chymotrypsin digests were carried out using a 1:5000 (mass:mass) ratio of protease to protein. Those with endoproteinase Glu were carried out using a 1:500 ratio. The protease concentrations were kept constant for the digests of the complex and those of Pap1 alone. For digests of the complex, a 1:1 molar ratio was formed with Fip1 at 0.5 mg/mL and Pap1 at 2.5 mg/mL. For the Pap1 alone digests, the Pap1 concentration was 2.5 mg/mL. All proteins were digested at 4 °C. Aliquots were taken after 10 min, 20 min, 80 min, 5 h, and 22 h. All proteolysis reactions were stopped by pipetting aliquots into hot SDS loading buffer, and the aliquots were analyzed by SDS−PAGE. Circular dichroism was measured using a Jasco J-810 spectropolarimeter with a 0.1 cm cuvette. A 6 μM Fip192 sample was prepared by diluting the stock protein 600-fold into 5 mM Tris, pH 7.5. Measurements for background correction were made by subtracting the buffer signal. The CD instrument was equipped with thermostated cell holders set to 20 °C. The CD unfolding experiment was performed by monitoring 208 nm from 5 to 90 °C, at a rate of 1 °C/min. The reference spectra shown in the figure were taken from the Supporting Information of Poschner et al. (*33*). Isothermal titration calorimetry (ITC) experiments were carried out on a MicroCal VP-ITC titration calorimeter using the VPViewer software for instrument control and data acquisition. The buffer used for the ITC experiments contained 10 mM phosphate, pH 6.8, 75 mM NaCl, 2 mM $MgCl_2$, 1 mM DTT, and 10% glycerol. Both purified proteins were dialyzed extensively in the same container at 4 °C against this buffer. Both samples were degassed prior to use. During the titration experiment, a 1 μM solution of PAP was held at 30 °C in a stirred reaction cell of 1.4 mL, and injections were made of a 10 μM solution of Fip1. Biacore affinity measurements were made using a Biacore 3000 surface plasmon resonance (SPR) instrument (Biacore, Piscataway, NJ). Details regarding this experiment are provided in the Supporting Information.

RESULTS

Structure of the Pap1/Fip$_{pbd}$ Complex. The structure of Pap1 in complex with a peptide containing residues 80−105 of Fip1 was determined by molecular replacement, using the structure of yeast Pap1 as a search model. This fragment was pursued after extensive efforts to crystallize a series of longer Fip1 constructs either alone or in complex with Pap1. The structure was refined to 2.6 Å resolution (Table 1), and there are two stereochemically similar Pap1/Fip$_{pbd}$ complexes in the asymmetric unit of the crystals. Crystals of the Pap1/Fip$_{pbd}$ complex were grown without substrates in the active site, and both of the Pap1 molecules in this new crystal form are in intermediately closed states relative to earlier Pap1 structures. Electron density for the Fip1 peptide was clearly evident after the initial molecular replacement, and a simulated annealing omit map of the region containing Fip1 is presented in Figure 1a. Each molecule of Pap1 was found to bind a molecule of 2-(*N*-morpholino)ethanesulfonic acid (MES), which was used as a buffer in the crystallization drop. The MES binding site is far removed from that of Fip1$_{pbd}$ and is unlikely to have any significant effect on the Pap1−Fip1$_{pbd}$ interface. Water molecules and ordered glycerol, which was used as a cryoprotectant, were also modeled into the electron density maps.

Fip$_{pbd}$ binds the outside face of the Pap1 C-terminal domain at a site well removed from the large, central cleft

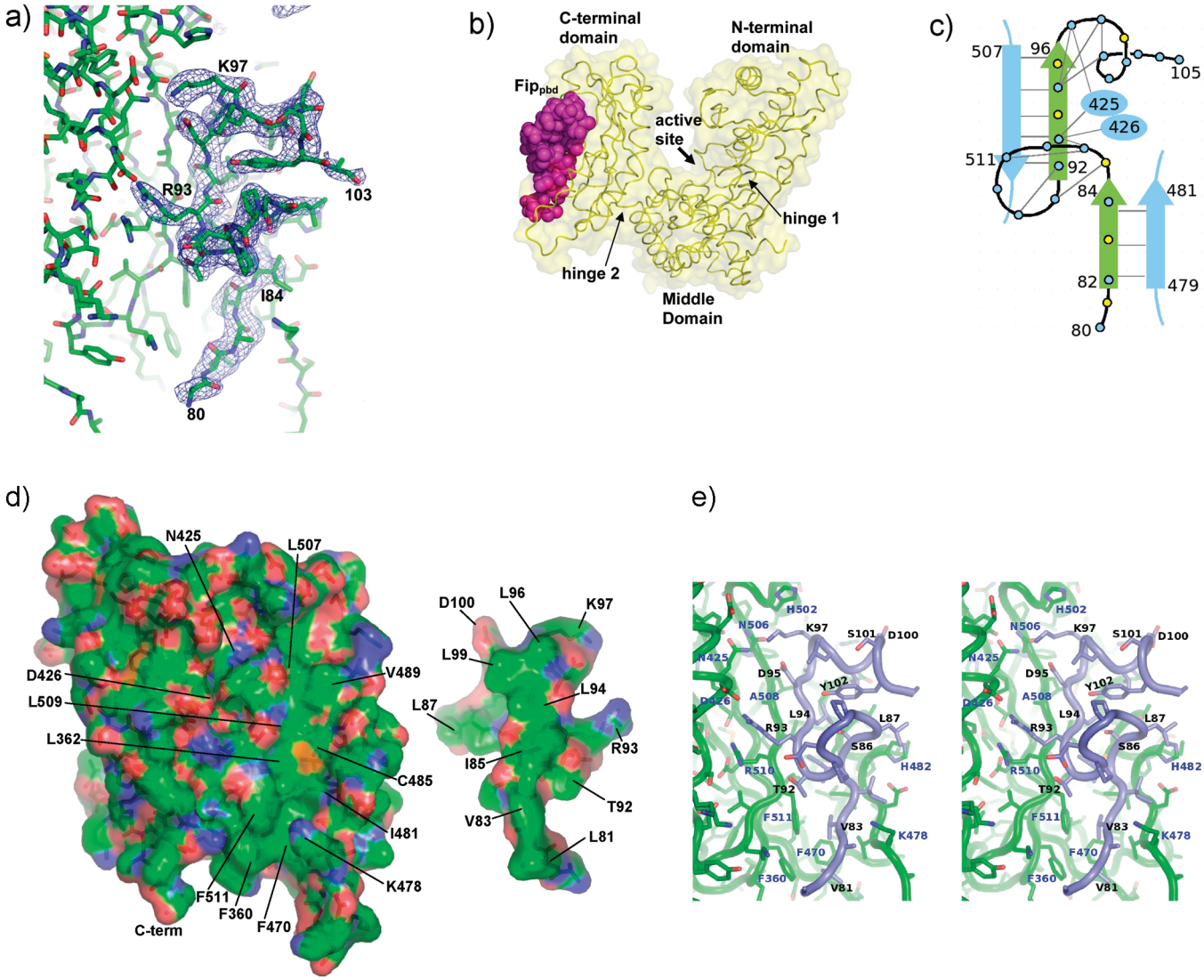

FIGURE 1: Structure of the Pap1−Fip$_{pbd}$ complex. (a) The simulated annealing omit map of Fip$_{pbd}$ calculated in CNS (*43*) and contoured at 3σ. Electron density for residues at both termini was weak, and side chain atoms beyond the α carbon were not built into the model for these residues. The central portion of the peptide exhibited unambiguous density. (b) Structure of the Pap1/Fip1 complex with Fip$_{pbd}$ shown in purple. In this view, the central, substrate-binding cleft of Pap1 is clearly visible. Arrows denote the location of the active site and the approximate locations of the two hinge regions. In the closed, RNA-bound complex, the three domains move with respect to one another via these hinges and the upper parts of the palm and C-terminal domains contact one another, encircling the single-stranded RNA. There is no overlap between the substrate-binding site and that of Fip$_{pbd}$. (c) Schematic diagram showing hydrogen-bonding interactions within Fip1 and between Fip1 and Pap1. The hydrophobic residues that interact with Pap1 are marked with yellow circles. (d) Surface representation of the Pap1 C-terminal domain (left) and Fip1$_{pbd}$ (right). The view of Pap1 is rotated approximately 90° about the vertical axis relative to (a), such that the view is of the face of Pap1 to which Fip1 is bound. Fip1 has been removed and rotated such that the right part of the figure shows the face of Fip1 which Pap1 is bound. The surface has been colored according to atom type (green = carbon, red = oxygen, blue = nitrogen, and yellow = sulfur) so as to highlight the hydrophobicity of both halves of the interface. (e) Stereoview of the complex. Pap1 is shown in green with labels in blue. The Fip$_{pbd}$ peptide is shown in blue, with black labels. The Pap1 residues mutated to disrupt the interface are mostly hidden behind Fip$_{pbd}$ in this view. V489 lies directly beneath the side chain hydroxyl of Y102. C485 is behind the main chain segment from I85 to S86.

that is responsible for Pap1 substrate binding and catalysis (Figure 1b). Fip1$_{pbd}$ does not interact with either of the Pap1 hinge regions, and as discussed below, neither the structure nor our kinetic measurements suggest that Fip1 binding alters Pap1 flexibility or hinders the domain movements to any significant degree. Fip$_{pbd}$ also does not occlude the ends of the central, substrate-binding cleft, which is formed by the inside faces of the three Pap1 domains. This is important because one end of this channel is required for egress of the elongating mRNA strand, and the opening at the other end of channel may facilitate ATP binding and pyrophosphate release. Except for the relatively small differences discussed below, the structure of the Pap1 C-terminal domain is quite similar to that observed in crystal structures without Fip1.

It is not uncommon to see that tight-binding complexes exhibit greater structural order than their uncomplexed states, and this appears to be the case with Pap1. In the four earlier Pap1 crystal structures (*4, 7, 34*) (with six crystallographically unique molecules) the C-terminal domain of the polymerase always exhibited higher *B*-factors than the other two domains. In contrast, *B*-factors in the Pap1/Fip1$_{pbd}$ complex are almost identical throughout, suggesting that Fip1 helps to stabilize the polymerase. The average *B*-factors for the two Fip1 peptides in this complex, however, are higher than that for

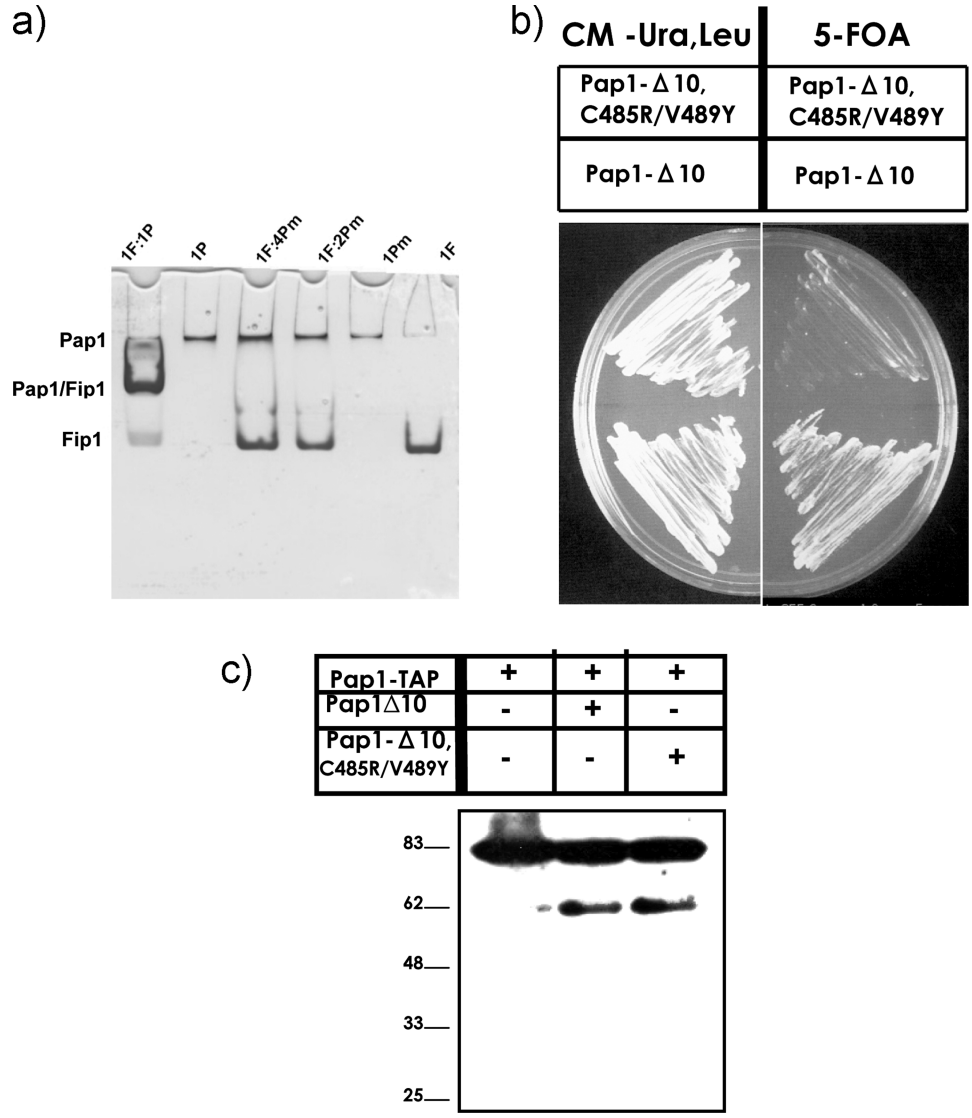

FIGURE 2: Characterization of the C485R/V489Y mutation in the Fip1 interaction domain of Pap1. (a) Lanes with the wild-type Pap1 enzyme are labeled P. Those with the double mutant are labeled Pm. F is used to denote Fip1. To form the complexes, 2.5 μg of bacterially expressed, purified Fip192 was combined with wild-type and mutant Pap1 at the stiochiometries indicated. Samples were run on a 10% polyacrylimide gel made at pH 8.8 using a Tris−borate buffer system. (b) Yeast containing a *PAP1* chromosomal deletion and the *PAP1* gene on a *URA3* plasmid were transformed with a *LEU2*+ plasmid containing the *PAP1-Δ10* or *pap1-Δ10,C485R/V489Y* allele. Transformants were grown on Complete media minus leucine and uracil (CM − Leu, Ura) or on media containing 5-fluoroorotic acid (5FOA), which forces loss of the *URA3* plasmid. Growth on 5FOA is observed only with cells containing *PAP1-Δ10*. (c) The pap1-Δ10,C485R/V489Y mutant protein is expressed in yeast at the same level as wild-type Pap1. Western blot was performed on extracts from cells expressing only a TAP-tagged Pap1 or the TAP-tagged Pap1 and either pap1-Δ10,C485R/V489Y or Pap1-Δ10 using a Pap1-specific antibody. The upper bands are the TAP-tagged Pap1. The lower ones are the native and mutant proteins without the TAP tag.

the Pap1 molecules, and both ends of the Fip1 peptide exhibited significant disorder.

Fip_{pbd} adopts a somewhat compact conformation when bound to Pap1. The structure of the peptide includes two loops (residues 85−91 and residues 97−103) that pack on either side of the Fip1 Y102 side chain. These loops are held together via a network of seven intramolecular hydrogen bonds (Figure 1c) involving both main chain and side chain atoms. The sidec hains of S86 and D90 appear to be particularly important, as both make hydrogen bonds to main chain atoms within the Fip1 peptide. However, neither these side chains nor the tyrosine at position 102 are well conserved, and even a search of the human Pap1 sequence for only the residues interacting with Fip1 failed to identify a region of clear homology. This suggests that the structure we observe may be unique to *Saccharomyces cerevisiae*.

The interface between Pap1 and Fip1 buries 1787 Å^2 of accessible surface area (966 Å^2 on Fip1 and 821 Å^2 on Pap1). The interface is dominated by two β strand interactions; Fip1 residues 82−84 form a parallel β ribbon with Pap1 residues 497−481, and Fip1 residues 92−96 form an antiparallel β sheet interaction with Pap1 residues 507−511. The former interaction involves Pap1 residues which are part of a large loop and are largely separate from the core of the C-terminal domain. This loop was usually poorly ordered in earlier Pap1 structures. The latter β strand interaction with Fip1 extends the central β sheet of the Pap1 C-terminal domain by an additional strand. There are eight hydrogen bonds between the β strands of Pap1 and Fip1. Fip1 makes three additional hydrogen bonds to Pap1; the side chain of R93 interacts with the carbonyl oxygens of Pap1 residues 425 and 426, and the side chain of K97 interacts with the side chain of

asparagine 425. Though Pap1 is a generally basic protein (pI = 7.95) electrostatics calculated with the programs PDB2PQR (*35*) and APBS (*36*) show that the surface to which these basic residues bind is acidic at neutral pH.

The side chain interactions between Pap1 and Fip1 are mostly through hydrophobic residues. Fip1 side chains L81, V83, I85, L94, L99, and A96 form a contiguous hydrophobic surface that is buried by the protein−protein interface. This interface has excellent shape complementarity with a contiguous hydrophobic surface on Pap1 involving residues F360, F470, F511, V479, I481, L362, C485, L509, V489, and L507 (Figure 1d). The conformation of these Pap1 residues is quite similar to that in Pap1 structures lacking Fip1; however, the hydrophobic residues in the earlier structures are somewhat buried by a helix composed of residues 482−494 and, in particular, by the R493 side chain. This helix ends two amino acids earlier in the Fip_{pbd} complex than in structures without Fip1. Also, the axis of this helix is tilted slightly in the Pap1−Fip1 complex, such that the new C-terminal end of helix at residue 492 is displaced by ~1.5 Å relative to structures without Fip1. In addition, the loop (from residues 493−498) which follows this helix adopts a different conformation, though it does not contact Fip_{pbd}. Overall, the changes in Pap1 that result from Fip_{pbd} binding are relatively small. Thus, most of the protein−protein interface we describe here is exposed to solvent in the structures of Pap1 lacking the Fip1 peptide. Coordinate files containing all of the Pap1 structures (six models without Fip1 and two models with Fip_{pbd}) with their C-terminal domains superimposed are provided as Supporting Information.

A Pap1 Mutant Abrogates Fip1 Binding in Vitro and Shows a Lethal Phenotype in Vivo. To further validate the structure of the complex and confirm that the interface we observe includes the most important epitope of binding between Pap1 and Fip1, we used the crystal structure to design a Pap1 mutant that disrupts Fip1 binding. The surface on Pap1 to which Fip1 binds is concave, and aside from its hydrophobicity, it has few distinguishing features. Since alanine mutants on such a surface might easily be tolerated, we chose to disrupt the interaction by replacing two relatively small side chains near the center of the interacting surface with more bulky ones. Val489, which interacts with Fip1 residues Leu94, Leu99, and Ala96, was mutated to tyrosine. Cys485, which contacts Ile85 and Leu94 on Fip1, was mutated to arginine. The double mutant, V498Y C485R, was first expressed in bacteria and purified in the same manner as the wild-type enzyme. Perhaps because these mutations reduce the predicted hydrophobicity of the Pap1 surface, the protein exhibited very good solubility, and the yields were somewhat higher than those obtained from the equivalent enzyme construct lacking the mutations. As the Fip1-binding site is far removed from the active site of Pap1, we were not surprised to find that the mutant exhibited wild-type polyadenylation activity (data not shown). To assess Fip1 binding, we performed a gel shift experiment (Figure 2a). In this experiment, Pap1 does not enter the gel because it is positively charged. Uncomplexed Fip1 migrates farthest, and the complex shows an intermediate band. Whereas wild-type Pap1 retards virtually all of the Fip1 when mixed at 1:1 stochiometry, the mutant shows no evidence of complex formation, even when Pap1 is in 4-fold molar excess over Fip1.

To investigate the effect of this mutation *in vivo*, the Val498Y C485R mutation of Pap1 was introduced into yeast using a plasmid shuffling strategy. Consistent with earlier work demonstrating that deletion of the Pab1-binding domain of Fip1 is lethal (*11*), yeast which were forced to express the mutant Pap1 molecule in place of the equivalent wild-type construct were unable to survive (Figure 2b). As shown in Figure 2c, the protein size and expression levels within yeast of the plasmid-expressed wild-type and mutant molecules were similar, confirming that the lethality is related to the mutated interface and not a defect in Pap1 expression or stability. We anticipate that the mutant described here will be useful in future studies, as it allows the Pap1−Fip1 interface to be disrupted with only a minor change in the Pap1 molecule.

Isolated Fip1 Is Monomeric, Highly Elongated, and Lacking in Large, Structured Domains in the Absence of Other Proteins. Recombinant full-length Fip1 is known to run significantly larger than its calculated molecular mass when subjected to gel filtration, and it had been suggested that this is due to the proline-rich region at the protein's C-terminal end which is most likely disordered (*10*). We found, however, that even Fip1 truncations lacking the proline-rich region (i.e., those ending at residues 192 and 220, referred to here as Fip192 and Fip220, respectively) still run at roughly three times their expected molecular mass by gel filtration. The Fip1 proteins elute well after the void volume of the column, so the high molecular mass observed cannot be attributed to simple protein aggregation. Gel filtrations runs of the Pap1−Fip1 complex also suggested an anomalously large molecular mass. For instance, the 83 kDa Pap1−Fip192 complex has an apparent molecular mass of 190 kDa. Consistent with these data, dynamic light scattering indicates that the purified proteins have a much larger physical size than would be expected if they adopted a globular structure. As shown in Figure 3a, isolated Fip192 (22 kDa) appears to have a radius approximately 10% larger than that of Pap1 (61 kDa), and the complex of the two proteins is larger still. DLS also indicates that purified Fip1 constructs and Fip−Pap1 complexes are generally monodisperse, suggesting that there is a uniform distribution of molecular size in solution.

To determine if Fip1 forms dimers or higher order complexes, we conducted a sedimentation velocity analytical ultracentrifugation (AUC) experiment on the Fip220 protein (Figure 3b). This construct supports wild-type levels of growth when introduced into yeast cells (*11*), but it lacks the proline-rich region near the C-terminus and is less prone to proteolysis during expression than the full-length construct. The AUC experiments yielded a molecular mass of 24.5 ± 0.2 kDa (CL 0.95) very close to the formula weight (25.5 kDa). This clearly indicates that Fip1 is a monomer in solution. The sedimentation coefficient ($s_{20,w}$ = 1.662 ± 0.002 S (CL 0.95)) and molar mass give a frictional ratio of 1.59 after taking 0.4876 g of water/g of protein into account, indicating that the molecule is extremely elongated. The hydrodynamically equivalent prolate ellipsoid has an axial ratio, a/b, of approximately 11.9. Thus, the observed sedimentation coefficient is consistent with the idea of a highly extended protein. The 1.66 S value we measured suggests, however, that Fip1 may not be completely extended. A fully random coil of molar mass 24.4 kDa would

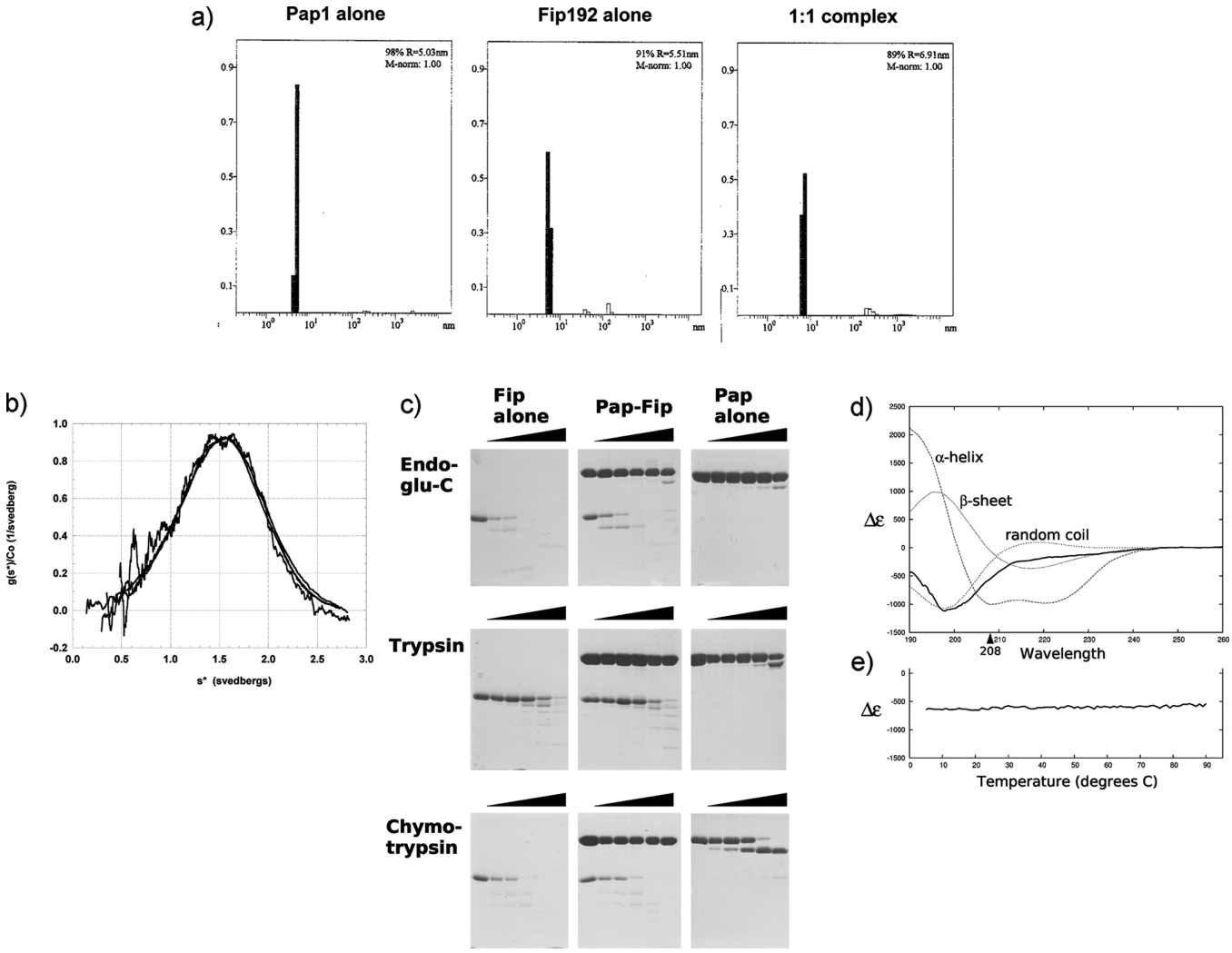

FIGURE 3: Biochemical and biophysical studies of Fip1 and the Fip1−Pap1 complex. (a) Dynamic light scattering results from Pap1 alone, Fip192 alone, and a 1:1 complex of the proteins demonstrate that Fip1 has larger radius than would be expected of a protein of this size and that neither the protein alone nor the Pap1−Fip1 complex forms aggregates. (b) Analytical ultracentrifugation of Fip220. Data from four solutions of Fip1 (at 1.15, 0.38, 0.138, and 0.044 mg/mL) are shown. (c) Proteolysis of Fip1, the Pap1−Fip1 complex, and Pap1 alone with endoproteinase Glu C, trypsin, and chymotrypsin. For each protein or complex the undigested sample is followed by five time points during the course of the digestion. Samples were taken after 8 min, 20 min, 80 min, 5 h, and 22 h. (d) Circular dichoism spectrum of Fip192. Theoretical spectra of pure α-helix, *β*-sheet, and random coil are shown for comparison. (e) Circular dicroism melting curve of Fip192 taken at 208 nm.

have a sedimentation coefficient of 0.99 S, whereas a completely spherical protein of this molar mass would have a sedimentation coefficient of 1.89 S.

To further probe the extended nature of Fip1, we subjected the purified protein to limited proteolysis. Figure 3c shows the digestion time course of Fip1, the Pap1−Fip1 complex, and Pap1 alone when they are incubated with endoproteinase Glu C, trypsin, and chymotrypsin. Preliminary experiments involving endoproteinase Lys C and elastase gave similar results (data not shown). Under conditions where we normally observe cleavage of flexible linker regions between domains and of floppy ends of otherwise structured proteins, Fip1 yielded no domain-sized stable digestion fragments. Also, the digestion of Fip1 was almost identical with and without Pap1. Thus, in spite of the tight binding between these proteins (discussed below) Pap1 does not appear to protect Fip1 from the various proteases. Notably, the converse is not true. Whereas Pap1 does not protect Fip1 from proteolysis, Fip1, even though it appears to be completely digested, does protect Pap1 from proteolysis by trypsin and chymotrypsin. These data suggest that a fragment or fragments of Fip1 too small to be visualized on the gels bind tightly to Pap1 and stabilize the structure of the polymerase. This interpretation is wholly consistent with the crystallographic observations involving the Fip1-induced ordering of the Pap1 C-terminal domain.

To probe the secondary structure of the elongated conformation adopted by Fip1, we examined the circular dichoism spectrum (Figure 3d). The spectrum is generally consistent with that of a random coil, though the absence of a positive signal around 220 nm suggests the possibility of a small helical component. To test this, we performed a CD melting experiment at 208 nm, a wavelength where α helices produce a strong signal. As shown in Figure 3e, the CD signal was virtually unchanged as the Fip1 sample was slowly heated from 5 to 90 °C. When globular proteins reach their melting temperature, they typically exhibit a well-defined transition in their CD spectra. As no such transition was observed, we conclude that Fip1, while highly soluble,

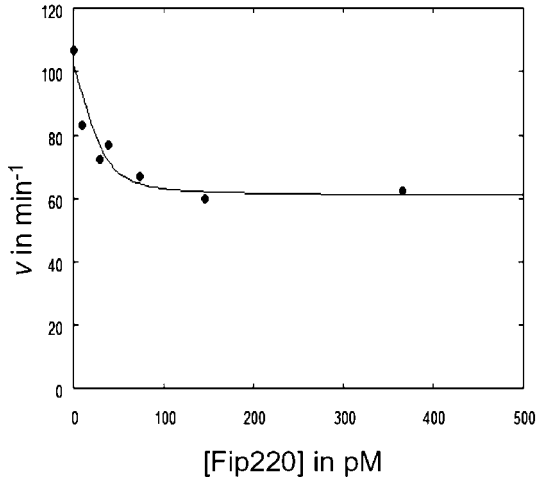

FIGURE 4: Determination of PAP-Fip binding constant by inhibition kinetics. The initial velocity was plotted as a function of Fip220 concentration, and the data were analyzed according to a model describing partial, tight-binding inhibition. The experiment included 36 pM PAP, 120 μM MgATP, 53 μM A_{18}, and 10 mM $MgCl_2$. Fip220 was added up to a 10-fold molar excess over Pap1. The apparent maximal velocity was determined to be 102.3 min^{-1} ($\pm$4%), the apparent velocity of the PAP−Fip220 complex is 60.6 min^{-1} ($\pm$16%), and the K_d is 4.4 pM ($\pm$126%).

is mostly, if not completely, disordered in the absence of its binding partners.

Inhibition of Pap1 by Fip1 and the Affinity of the Pap1−Fip1 Interaction. We measured the affinity of Pap1 for both the Fip1 protein and a Fip1 peptide including the 80−105 region. A previous report (*11*) indicated a Fip1-induced decrease in Pap1 activity, and we used this to measure the binding of Pap1 to Fip220. Consistent with the earlier work, we show that binding of Fip1 to Pap1 causes a decrease in polyadenylation activity (Figure 4a). The velocity of polyadenylation was measured at a single concentration of MgATP and an oligo(A) 18mer (both near their respective K_ms) as a function of Fip220 concentration in the range of 0−365 pM. Two results are immediately apparent. First, Fip220 exhibits tight binding (K_d = 4.4 pM). This is consistent with the high-affinity binding observed by isothermal titration calorimetry (Supporting Information Figure 1). Second, the inhibition of PAP by Fip is partial; the PAP−Fip complex retains about 60% of the activity of PAP alone, under the present assay condition. Partial inhibition was also seen previously (*11*). In that case, a 20-fold effect on the "K_m" for the RNA substrate was reported. We also confirmed that the effect is competitive with respect to RNA (not shown), but our experiment shows a more modest (~3-fold) effect, apparently owing to differences in assay conditions. Similar results were obtained with Fip192, although in that case, while the binding is still very tight, the inhibitory effect on Pap1 at saturating concentrations of Fip1 was even less pronounced (data not shown). These results are consistent with the disordered terminal regions of Fip interfering with, but not preventing, RNA binding to the active site. We suggest the interference is due to steric effects, though our result is equally consistent with Fip inducing a small perturbation in the domain motion equilibrium such that Fip either stabilizes the open state or destabilizes the closed state. This sort of inhibition is not likely to be physiologically relevant, since the presence of RNA at a high local concentration, as is expected when the RNA substrate is tethered to the polymerase within the biological complex, would completely relieve the inhibition. Additionally, the N- and C-terminal regions of Fip, which are disordered in this system, are very likely to be engaged in other protein−protein interactions *in vivo*. Indeed, the earlier study reported that the inhibition of Pap1 by Fip1 is relieved in the context of the larger complex (*11*).

The Fip_{pbd} peptide does not inhibit Pap1 activity even at concentrations in excess of 200 μM (data not shown). The peptide yields clear gel shifts in experiments analogous to those presented in Figure 2a, but since accurate quantitation of such gel-based experiments is difficult, we used surface plasmon resonance to characterize the affinity of Pap1 for $Fip1_{pbd}$. A biotinylated $Fip1_{pbd}$ peptide was coupled to a streptavidin chip, and a series of Pap1 solutions at varying concentrations were injected into the apparatus. The resulting sensorgrams yielded a K_d value of 3 μM (Supporting Information Figure 2). As longer versions of Fip1 bind Pap1 significantly more tightly, it appears that residues outside of the 80−105 region of Fip1 serve to enhance the interaction we describe structurally.

There are multiple alternative explanations for the difference in binding we observe: Full-length Fip1 may undergo energetically favorable internal rearrangements upon Pap1 binding that significantly augment the binding energy. Biotinylation of the Fip1 peptide may have partially interfered with Pap1 binding, or regions of Fip1 which normally interact with other parts of the polyadenylation complex may bind instead to Pap1 when experiments are performed on the isolated proteins. Any of these factors, or some combination thereof, could contribute. Because Fip1 is known to interact with other proteins within the polyadenyation complex, we anticipate that the biologically relevant affinity measurements will likely only be observed in the context of the macromolecular assembly. Unfortunately, stoichiometrically uniform preparations of the complex with all of the Fip1-interacting proteins have not yet been achieved, and quantitative measurements of this sort are impossible at this time.

In evaluating the importance of the Fip_{pbd} region it is important to keep in mind that this region was originally identified in an earlier study wherein progressive deletions from either side of Fip1 were characterized with respect to their effect on Pap1 binding and yeast viability. Fip1 lacking the Fip_{pbd} region resulted in a lethal phenotype and exhibited no detectable Pap1 binding (*11*). Herein we have shown that the Fip_{pbd} peptide binds Pap1 with reasonable affinity and that disruption of even part of the Pap1−Fip_{pbd} interface (via the V498Y, C485R mutant of Pap1) causes a total loss of wild-type Fip1 binding. Thus, we believe that the interaction we have characterized through our structural work is likely to be the primary binding determinant between Pap1 and Fip1. Additional binding sites may exist, but these are insufficient to bring Pap1 and Fip1 together in the absence of the interactions involving the Fip_{pbd} region.

Residues at the Pap1 Fip_{pbd} Interface Are Poorly Conserved. The C-terminal domains of yeast and mammalian PAP have similar three-dimensional structures, but whereas the N-terminal and middle domains share 47% sequence identity, the C-terminal domains are only 24% identical. Surprisingly, the Pap1 residues mediating the Pap1−Fip_{pbd} interaction were no more conserved from yeast to mammals

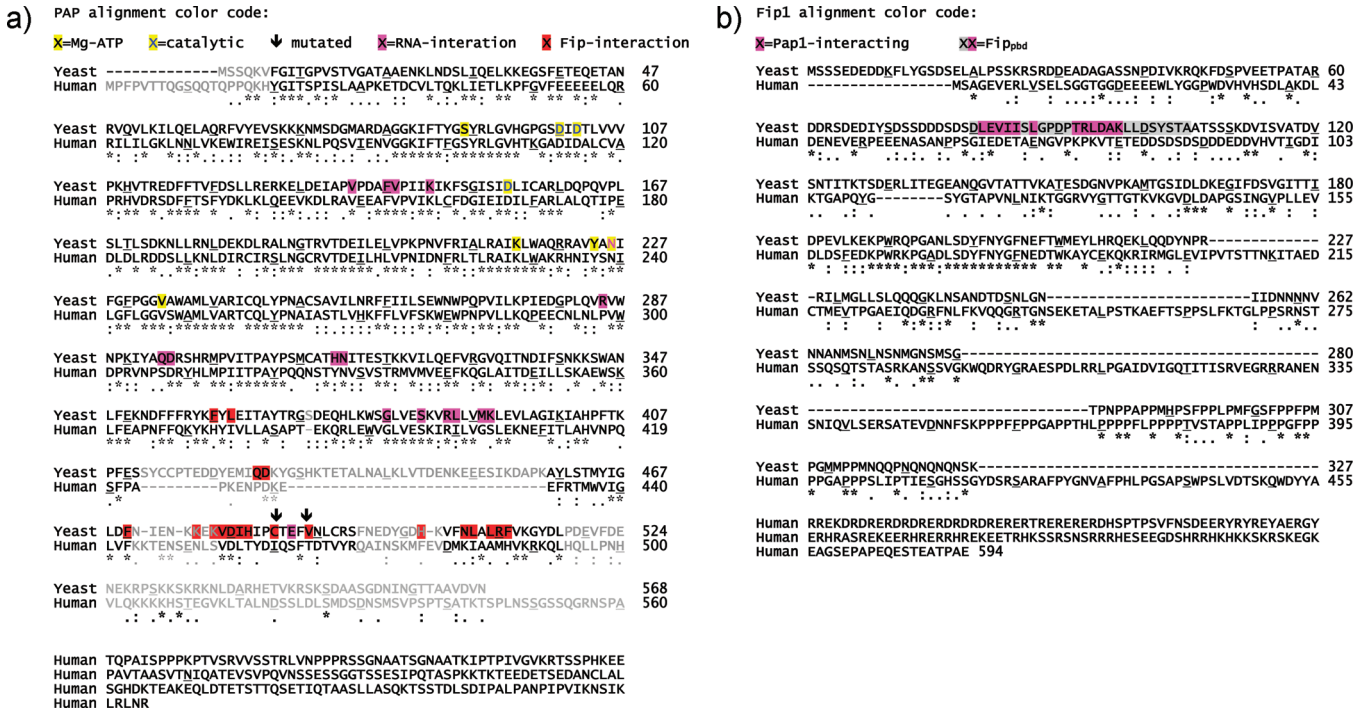

FIGURE 5: Sequence alignments between yeast and human Pap1 and Fip1. (a) Pap1 structure-based sequence alignment. Residues contacting Fip1 are colored red. To distinguish these from other functionally important residues, residues involved in Mg-ATP binding have been highlighted in yellow, and those shown to bind RNA are highlighted in magenta. Arrows denote the two residues mutated to abrogate Fip1 binding. Residues shown in gray are in significantly different conformations in structures of yeast and bovine PAP. Any sequence conservation within these regions is unlikely to be of functional significance. (b) Fip1 alignment. The region corresponding to the Fip$_{pbd}$ is colored gray, with those residues contacting Pap1 colored magenta. The entire length of each sequence is shown to highlight the lack of sequence conservation in the region corresponding to our peptide.

than the rest of the C-terminal domain (Figure 5a). In fact, the contacts involving yeast PAP residues 425 and 426 are located in a 36 amino acid insertion in the yeast PAP sequence relative to that of the human enzyme. This insertion forms two α helices and a connecting loop which sit on one side of the Fip1-binding surface. Even in structures from crystals of yeast Pap1 grown without Fip1, the Fip1-binding site appears as a hydrophobic groove at the protein surface. In contrast, crystal structures of bovine PAP (*5, 6*) reveal no obvious groove and a much more hydrophilic surface at this site.

Homology between yeast and human Fip1 sequences is also very limited, and the low sequence homology among the residues corresponding to the Fip$_{pbd}$ suggests that the molecular details of the Pap/Fip interaction may not be conserved (Figure 5). Human Fip1 and human PAP are, however, known to interact. Furthermore, deletion studies have demonstrated that the first 111 amino acids of human Fip1 (which includes the region most homologous to Fip$_{pbd}$) are sufficient for PAP binding. These studies also show that affinity for PAP is increased if the human Fip1 sequence is extended to residue 355 (*19*). Thus, the same general region of Fip1 may be involved in PAP binding in both cases.

Though perhaps counterintuitive, the idea that an interaction between PAP and Fip1 is conserved across the phyla, but the atomic details of this interaction are not, is consistent with one other piece of data. In a background deficient in both Pap1 and Fip1, yeast are rescued by a Pap1−Fip1 fusion with full-length Pap1 followed by residues 91−327 of Fip1 (data not shown). This construct lacks the N-terminal β strand of Fip1$_{pbd}$ and the hydrophobic, Pap1-interacting residues at positions 81, 83, and 85. Thus, the connection between Pap1 and Fip1 in this construct is significantly different from that observed in our structure. Like the sequence data presented above, this yeast rescue suggests that while tethering Pap1 to Fip1 is essential, the molecular details of tethering are not crucial.

Table 1: Data Collection and Refinement Statistics[a]

Data Collection	
radiation source	NSLS beamline X29a
space group	$P2_12_12$
cell dimensions (Å; deg)	111.124, 184.211, 73.534; 90, 90, 90
R_{merge} (%)	10.6 (48.0)
$I/\sigma I$	23.09 (2.11)
completeness (%)	99.6 (96.4)
redundancy	10.0 (9.7)
Refinement	
resolution (Å)	2.6
no. of reflections	46949
R_{work} (%)/R_{free} (%)	19.72/25.82
no. of protein atoms	8866
no. of water atoms	210
no. of glycerol/MES atoms	102
rmsd, bond lengths (Å)	0.011
rmsd, bond angles (deg)	1.477
Ramachandran plot	
most favored/allowed (%)	99.6 (981 residues)
generously allowed (%)	0.4 (4 residues)
disallowed regions (%)	0.0 (0 residues)

[a] Highest resolution shell is shown in parentheses.

SUMMARY AND CONCLUSIONS

The crystal structure we present shows that Fip$_{pbd}$ binds to a hydrophobic channel on the surface of the C-terminal domain of Pap1 and that this interaction does not interfere

with Pap1's domain movements or with the polymerase's central, substrate-binding cleft. These observations are supported by the kinetics of Fip1's inhibition of Pap1 activity; Fip1 exhibits only a modest effect on catalysis, and as noted above, we believe it likely that this reduction in polyadenylation activity is relieved by the presence of other domains within the complex which interact with the otherwise disordered regions of Fip1 and perhaps also by the locally high concentration of RNA present in the active polyadenylation complex. Thus, Fip1-mediated downregulation of Pap1 activity in the yeast system is most likely not a *bona fide* mechanism of poly(A) tail length regulation. Termination of polyadenylation may instead be mediated by reversible posttranslational modifications as has been more recently proposed (*37, 38*). Likewise, the increase in Pap1 activity by Fip1 seen in the mammalian and *Arabidopsis* systems can be explained by the fact that, unlike yeast, these Fip1 proteins contain RNA-binding domains; such domains serve to tether the polymerase to its substrate and increase the observed activity (*19, 20*).

The yeast protein Fip1 is largely disordered in the absence of Pap1, and the results presented here suggest that only a portion of Fip1 folds upon binding the polymerase. Thus, Fip1 exhibits all of the characteristics of a natively unfolded protein; though it is extremely soluble and monomeric, it is highly susceptible to proteolysis, and it exhibits an anomalously large molecular mass when characterized by gel filtration or dynamic light scattering. Intrinsically disordered proteins have been reported with increasing frequency, and such proteins are now believed to encompass a significant fraction of the eukaryotic proteome (*39–41*). It has been suggested that the extended nature of intrinsically disordered scaffolding proteins facilitates interaction with multiple binding partners via a limited number of amino acids (*42*). This may help to explain the seemingly curious nature of Fip1.

The structure of Fip1 when bound to other factors within the cleaveage/polyadenylation apparatus is unknown, but we are inclined to believe that Fip1 flexibility is at least partially maintained in the context of the larger complex. An intrinsically flexible Fip1 molecule might help to explain why Fip1 is so poorly conserved across the phyla; residues that serve as linkers need not be conserved, and if the protein lacks a hydrophobic core, there are far fewer constraints on its sequence. The prospect of having Pap1 attached to the complex via a flexible linker is also attractive from a structural standpoint, as it would allow Pap1 ample space for the large-scale domain movements that it undergoes during its catalytic cycle (*34*). Additional work is clearly needed to determine if interactions with other polyadenylation subunits induce further order upon Fip1. The molecular details of these interactions may have diverged across species, but it is likely that the general themes of Fip1 function are conserved; a portion of Fip1 tethers the polymerase to the processing complex in a way which does not impinge on catalytic function, while other portions of Fip1 connect PAP to its RNA substrate, either directly, as in human Fip1, or via other RNA-binding subunits of the complex, as in yeast Fip1. In both cases, the ultimate goal is to facilitate the rapid synthesis of the poly(A) tail.

ACKNOWLEDGMENT

We thank Howard Robinson at NSLS for collecting the diffraction data, Eunhee Lee for assistance with the analytical ultracentrifugation, Gillian Henry for help with the circular dichroism experiments, Eric Sundberg for help with the Biacore experiment, and Alexander Zhelkovsky for useful discussions.

SUPPORTING INFORMATION AVAILABLE

The isothermal titration calorimetry data mentioned in the text and a discussion of the thermodynamics of Pap1/Fip1 binding are presented. The surface plasmon resonance results involving Pap1 and the Fip_{pbd} peptide are also presented. Pap1 PDB files for the six crystallographically independent Pap1 molecules in the absence of Fip1 and the two molecules in the presence of Fip_{pbd} are also available for download. The PDB files have all been oriented such that their C-terminal Pap1 domains are superimposed. Molecules 1A and 1B are from PDB code 1FA0, 2A and 2B are from 201P, 3A is from 2HHP, 4A is from 2Q66, and 5A and 5B are from the complex presented here. This material is available free of charge via the Internet at http://pubs.acs.org.

REFERENCES

1. Zhao, J., Hyman, L., and Moore, C. (1999) Formation of mRNA 3′ ends in eukaryotes: mechanism, regulation, and interrelationships with other steps in mRNA synthesis. *Microbiol. Mol. Biol. Rev. 63*, 405–445.
2. Gilmartin, G. M. (2005) Eukaryotic mRNA 3′ processing: a common means to different ends. *Genes Dev. 19*, 2517–2521.
3. Aravind, L., and Koonin, E. V. (1999) DNA polymerase beta-like nucleotidyltransferase superfamily: identification of three new families, classification and evolutionary history. *Nucleic Acids Res. 27*, 1609–1618.
4. Bard, J., Zhelkovsky, A. M., Helmling, S., Earnest, T. N., Moore, C. L., and Bohm, A. (2000) Structure of yeast poly(A) polymerase alone and in complex with 3′-dATP. *Science 289*, 1346–1349.
5. Martin, G., Keller, W., and Doublie, S. (2000) Crystal structure of mammalian poly(A) polymerase in complex with an analog of ATP. *EMBO J. 19*, 4193–4203.
6. Martin, G., Moglich, A., Keller, W., and Doublie, S. (2004) Biochemical and structural insights into substrate binding and catalytic mechanism of mammalian poly(A) polymerase. *J. Mol. Biol. 341*, 911–925.
7. Balbo, P. B., Toth, J., and Bohm, A. (2007) X-ray crystallographic and steady state fluorescence characterization of the protein dynamics of yeast polyadenylate polymerase. *J. Mol. Biol. 366*, 1401–1415.
8. Balbo, P. B., Meinke, G., and Bohm, A. (2005) Kinetic studies of yeast polyA polymerase indicate an induced fit mechanism for nucleotide specificity. *Biochemistry 44*, 7777–7786.
9. Balbo, P. B., and Bohm, A. (2007) Mechanism of Poly(A) Polymerase: Structure of the enzyme-MgATP-RNA ternary complex and kinetic analysis, Structure. (in press).
10. Preker, P. J., Lingner, J., Minvielle-Sebastia, L., and Keller, W. (1995) The FIP1 gene encodes a component of a yeast pre-mRNA polyadenylation factor that directly interacts with poly(A) polymerase. *Cell 81*, 379–389.
11. Helmling, S., Zhelkovsky, A., and Moore, C. L. (2001) Fip1 regulates the activity of Poly(A) polymerase through multiple interactions. *Mol. Cell. Biol. 21*, 2026–2037.
12. Dheur, S., Nykamp, K. R., Viphakone, N., Swanson, M. S., and Minvielle-Sebastia, L. (2005) Yeast mRNA Poly(A) tail length control can be reconstituted in vitro in the absence of Pab1p-dependent Poly(A) nuclease activity. *J. Biol. Chem. 280*, 24532–24538.
13. Ohnacker, M., Barabino, S. M., Preker, P. J., and Keller, W. (2000) The WD-repeat protein pfs2p bridges two essential factors within the yeast pre-mRNA 3′-end-processing complex. *EMBO J. 19*, 37–47.

14. Barabino, S. M., Hubner, W., Jenny, A., Minvielle-Sebastia, L., and Keller, W. (1997) The 30-kD subunit of mammalian cleavage and polyadenylation specificity factor and its yeast homolog are RNA-binding zinc finger proteins. *Genes Dev. 11*, 1703–1716.
15. Gross, S., and Moore, C. L. (2001) Rna15 interaction with the A-rich yeast polyadenylation signal is an essential step in mRNA 3′-end formation. *Mol. Cell. Biol. 21*, 8045–8055.
16. Ryan, K., Calvo, O., and Manley, J. L. (2004) Evidence that polyadenylation factor CPSF-73 is the mRNA 3′ processing endonuclease. *RNA (New York, NY) 10*, 565–573.
17. Zhelkovsky, A., Tacahashi, Y., Nasser, T., He, X., Sterzer, U., Jensen, T. H., Domdey, H., and Moore, C. (2006) The role of the Brr5/Ysh1 C-terminal domain and its homolog Syc1 in mRNA 3′-end processing in *Saccharomyces cerevisiae*. *RNA (New York, NY) 12*, 435–445.
18. Mandel, C. R., Kaneko, S., Zhang, H., Gebauer, D., Vethantham, V., Manley, J. L., and Tong, L. (2006) Polyadenylation factor CPSF-73 is the pre-mRNA 3′-end-processing endonuclease. *Nature 444*, 953–956.
19. Kaufmann, I., Martin, G., Friedlein, A., Langen, H., and Keller, W. (2004) Human Fip1 is a subunit of CPSF that binds to U-rich RNA elements and stimulates poly(A) polymerase. *EMBO J. 23*, 616–626.
20. Forbes, K. P., Addepalli, B., and Hunt, A. G. (2006) An Arabidopsis Fip1 homolog interacts with RNA and provides conceptual links with a number of other polyadenylation factor subunits. *J. Biol. Chem. 281*, 176–186.
21. Venkataraman, K., Brown, K. M., and Gilmartin, G. M. (2005) Analysis of a noncanonical poly(A) site reveals a tripartite mechanism for vertebrate poly(A) site recognition. *Genes Dev. 19*, 1315–1327.
22. McCoy, A., Grosse-Kunstleve, R. W., Adams, P. D., Winn, M. D., Storoni, L. C., and Read, R. J. (2007) Phaser crystallographic software. *J. Appl. Crystallogr. 40*, 658–674.
23. Emsley, P., and Cowtan, K. (2004) Coot: model-building tools for molecular graphics. *Acta Crystallogr. 60*, 2126–2132.
24. Murshudov, G. N., Vagin, A. A., and Dodson, E. J. (1997) Refinement of macromolecular structures by the maximum-likelihood method. *Acta Crystallogr. 53*, 240–255.
25. Winn, M. D., Isupov, M. N., and Murshudov, G. N. (2001) Use of TLS parameters to model anisotropic displacements in macromolecular refinement. *Acta Crystallogr. 57*, 122–133.
26. Lee, B., and Richards, F. M. (1971) The interpretation of protein structures: estimation of static accessibility. *J. Mol. Biol. 55*, 379–400.
27. DeLano, W. L. (2002)The PyMOL Molecular Graphics System.
28. Rothstein, R. J. (1983) One-step gene disruption in yeast. *Methods Enzymol. 101*, 202–211.
29. Sherman, F., Fink, G. R., and Hick, J. B. (1986) *Methods in yeast genetics*, Cold Spring Harbor Laboratory Press, Plainview, NY.
30. Kessler, M. M., Zhelkovsky, A. M., Skvorak, A., and Moore, C. L. (1995) Monoclonal antibodies to yeast poly(A) polymerase (PAP) provide evidence for association of PAP with cleavage factor I. *Biochemistry 34*, 1750–1759.
31. Stafford, W. F., and Sherwood, P. J. (2004) Analysis of heterologous interacting systems by sedimentation velocity: curve fitting algorithms for estimation of sedimentation coefficients, equilibrium and kinetic constants. *Biophys. Chem. 108*, 231–243.
32. Laue, T., Shah, B., Ridgeway, T., and Pelletier, S. (1992) *Computer-aided interpretation of analytical sedimentation data for proteins*, Royal Society of Chemistry, Cambridge, U.K.
33. Poschner, B. C., Reed, J., Langosch, D., and Hofmann, M. W. (2007) An automated application for deconvolution of circular dichroism spectra of small peptides. *Anal. Biochem. 363*, 306–308.
34. Balbo, P. B., and Bohm, A. (2007) Mechanism of Poly(A) Polymerase: Structure of the Enzyme-MgATP-RNA Ternary Complex and Kinetic Analysis. *Structure 15*, 1117–1131.
35. Dolinsky, T. J., Nielsen, J. E., McCammon, J. A., and Baker, N. A. (2004) PDB2PQR: an automated pipeline for the setup of Poisson-Boltzmann electrostatics calculations. *Nucleic Acids Res. 32*, W665–667.
36. Baker, N. A., Sept, D., Joseph, S., Holst, M. J., and McCammon, J. A. (2001) Electrostatics of nanosystems: application to microtubules and the ribosome. *Proc. Natl. Acad. Sci. U.S.A. 98*, 10037–10041.
37. He, X., and Moore, C. (2005) Regulation of yeast mRNA 3′ end processing by phosphorylation. *Mol. Cell 19*, 619–629.
38. Vethantham, V., Rao, N., and Manley, J. L. (2007) Sumoylation modulates the assembly and activity of the pre-mRNA 3′ processing complex. *Mol. Cell. Biol. 27*, 8848–8858.
39. Fink, A. L. (2005) Natively unfolded proteins. *Current Opin. Struct. Biol. 15*, 35–41.
40. Sugase, K., Dyson, H. J., and Wright, P. E. (2007) Mechanism of coupled folding and binding of an intrinsically disordered protein. *Nature 447*, 1021–1025.
41. Iakoucheva, L. M., and Dunker, A. K. (2003) Order, disorder, and flexibility: prediction from protein sequence. *Structure 11*, 1316–1317.
42. Gunasekaran, K., Tsai, C. J., Kumar, S., Zanuy, D., and Nussinov, R. (2003) Extended disordered proteins: targeting function with less scaffold. *Trends Biochem. Sci. 28*, 81–85.
43. Brunger, A. T., Adams, P. D., Clore, G. M., DeLano, W. L., Gros, P., GrosseKunstleve, R. W., Jiang, J. S., Kuszewski, J., Nilges, M., Pannu, N. S., Read, R. J., Rice, L. M., Simonson, T., and Warren, G. L. (1998) Crystallography & NMR system: A new software suite for macromolecular structure determination. *Acta Crystallogr. 54*, 905–921.

BI800204K